



UTE-T2* versus conventional T2* mapping to assess posterior cruciate ligament ultrastructure and integrity – an *in-situ* study

Lena Marie Wilms^{1,2^}, Karl Ludger Radke^{1^}, David Latz², Thomas Andreas Thiel^{1^}, Miriam Frenken¹, Benedikt Kamp^{1^}, Timm Joachim Filler^{3^}, Armin Michael Nagel^{4,5^}, Anja Müller-Lutz^{1^}, Daniel Benjamin Abrar^{1^}, Sven Nebelung^{1,6^}

¹Department of Diagnostic and Interventional Radiology, Medical Faculty, University Dusseldorf, Dusseldorf, Germany; ²Department of Orthopaedics and Trauma Surgery, Medical Faculty, University Dusseldorf, Dusseldorf, Germany; ³Institute for Anatomy I, Heinrich-Heine-University, Dusseldorf, Germany; ⁴Institute of Radiology, University Hospital Erlangen, Friedrich-Alexander-Universität Erlangen-Nürnberg (FAU), Erlangen, Germany; ⁵Division of Medical Physics in Radiology, German Cancer Research Center (DKFZ), Heidelberg, Germany; ⁶Department of Diagnostic and Interventional Radiology, University Hospital Aachen, Aachen, Germany

Contributions: (I) Conception and design: LM Wilms, S Nebelung; (II) Administrative support: LM Wilms, KL Radke, S Nebelung; (III) Provision of study materials or patients: LM Wilms, KL Radke, D Latz, AM Nagel, M Frenken, TJ Filler, A Müller-Lutz, DB Abrar, S Nebelung; (IV) Collection and assembly of data: LM Wilms, KL Radke, S Nebelung; (V) Data analysis and interpretation: LM Wilms, KL Radke, B Kamp, TA Thiel, S Nebelung; (VI) Manuscript writing: All authors; (VII) Final approval of manuscript: All authors

Correspondence to: Lena Marie Wilms, MD. Department of Diagnostic and Interventional Radiology, University Hospital Düsseldorf, Moorenstraße 5, 40225 Düsseldorf, Germany. Email: lena.wilms@med.uni-duesseldorf.de.

Background: Clinical-standard morphologic magnetic resonance imaging (MRI) is limited in the refined diagnosis of posterior cruciate ligament (PCL) injuries. Quantitative MRI sequences such as ultrashort echo-time (UTE)-T2* mapping or conventional T2* mapping have been theorized to quantify ligament (ultra-)structure and integrity beyond morphology. This study evaluates their diagnostic potential in identifying and differentiating partial and complete PCL injuries in a standardized graded injury model.

Methods: Ten human cadaveric knee joint specimens were imaged on a clinical 3.0 T MRI scanner using morphologic, conventional T2* mapping, and UTE-T2* mapping sequences before and after standardized arthroscopic partial and complete PCL transection. Following manual segmentation, quantitative T2* and underlying texture features (i.e., energy, homogeneity, and variance) were analyzed for each specimen and PCL condition, both for the entire PCL and its subregions. For statistical analysis, Friedman's test followed by Dunn's multiple comparison test was used against the level of significance of $P \leq 0.01$.

Results: For the entire PCL, T2* was significantly increased as a function of injury when acquired with the UTE-T2* sequence [entire PCL: 11.1±3.1 ms (intact); 10.9±4.6 ms (partial); 14.3±4.9 ms (complete); $P < 0.001$], but not when acquired with the conventional T2* sequence [entire PCL: 10.0±3.2 ms (intact); 11.4±6.2 ms (partial); 15.5±7.8 ms (complete); $P = 0.046$]. The PCL subregions and texture variables showed variable changes indicative of injury-associated disorganization.

Conclusions: In contrast to the conventional T2* mapping, UTE-T2* mapping is more receptive in the detection of structural damage of the PCL and allows quantitative assessment of ligament (ultra-)structure and integrity that may help to improve diagnostic differentiation of distinct injury states. Once further substantiated beyond the *in-situ* setting, UTE-T2* mapping may refine diagnostic evaluation of PCL injuries and -possibly- monitor ligament healing, ageing, degeneration, and inflammation.

[^] ORCID: Lena Marie Wilms, 0000-0002-1159-863X; Karl Ludger Radke, 0000-0003-1095-1283; Thomas Andreas Thiel, 0000-0002-2621-3958; Benedikt Kamp, 0000-0002-0518-5695; Timm Joachim Filler, 0000-0002-2922-5110; Armin Michael Nagel, 0000-0003-0948-1421; Anja Müller-Lutz, 0000-0002-7798-5384; Daniel Benjamin Abrar, 0000-0002-8116-4431; Sven Nebelung, 0000-0002-5267-9962.

Keywords: Magnetic resonance imaging (MRI); quantitative imaging; ultrashort echo-time (UTE)-T2*; posterior cruciate ligament (PCL); knee joint instability

Submitted Mar 17, 2022. Accepted for publication May 23, 2022.

doi: 10.21037/qims-22-251

View this article at: <https://dx.doi.org/10.21037/qims-22-251>

Introduction

The posterior cruciate ligament (PCL) is an essential stabilizer of the knee joint that restrains posterior translation of the tibia relative to the femur (1-4). Consequently, injuries of the PCL lead to posterior tibial subluxation, thus increasing the load on the posterior and posterolateral structures of the joint as well as on the medial femoral condyle (1-4). Without adequate and timely treatment, the resulting biomechanical alterations eventually lead to degenerative changes of the joint and, ultimately, post-traumatic osteoarthritis (2). As a result, nearly 80% of patients with chronic PCL deficiency suffer from irreversible cartilage damage (2). To prevent the development of post-traumatic osteoarthritis, timely and precise diagnosis of PCL injuries is vital. While diagnostic strategies are centred around the clinical examination and magnetic resonance imaging (MRI), PCL injuries are frequently missed in clinical practice (5,6). Because of complete fiber disruption, acute complete PCL injuries can be readily diagnosed using MRI with excellent sensitivity and specificity rates of $\geq 97\%$ (7-9). In contrast, the diagnosis of partial or chronic PCL injuries is challenging and suffers from poorer sensitivity and specificity rates as low as 62–67% (9-11). Due to traumatic stretching and elongation, the partially injured PCL is functionally insufficient (12), yet appears continuous or only slightly thickened on morphologic MRI (12,13). Because fiber thickening and edema slowly subside over time as the ligament scars, the chronically injured PCL is similarly challenging (14). Consequently, in 28% of patients with chronic PCL injuries, the ligament appears morphologically intact, too, without alterations in signal intensity (14,15). Thus, the extent of chronic PCL injury may be masked, leading to delayed or incorrect assessment and, eventually, unsatisfactory treatment outcomes (4).

Quantitative MRI techniques may overcome these diagnostic shortcomings by allowing ligament assessment beyond mere morphology. Wilson *et al.* used T2 mapping to highlight injured areas of the PCL and to differentiate

acute and chronic PCL injuries. In their pilot study of six patients with morphologically continuous, yet functionally insufficient PCLs, they found higher T2 relaxation times as compared to asymptomatic volunteers (16). Other studies consolidated the scientific evidence and investigated T2 mapping of the PCL in the context of osteoarthritis (17) and loading (18).

Conventional T2* mapping has been suggested as an alternative measure of ligament integrity because it may better capture the highly organized collagen structure and low water content (19). By accounting for B_0 inhomogeneity due to paramagnetic and diamagnetic effects, T2* is theorized to reflect the degree of collagen fibre orientation and alignment as well as the spin-to-spin interactions of protons bound to collagen (20,21). Consequently, T2* is widely considered a surrogate marker of ligament integrity and water content, collagen matrix organization, fibre orientation, and fibre alignment (19,20,22-24). Earlier studies used T2* mapping to evaluate the anterior cruciate ligament, menisci, and patellar tendon (19,24-27). For the PCL, data on T2* are scarce and only available for asymptomatic volunteers (22).

Ultrashort echo-time T2* (UTE-T2*) mapping is designed to image tissues with very short T2* relaxation times by capturing the signal before its decay (28). Theoretically, the technique may detect slighter changes in tissue (ultra-)structure than conventional T2* mapping (20). Using echo times as low as 0.5 ms, Hayashi *et al.* recently reported significantly higher T2* relaxation times in the PCLs of patients with osteoarthritis as compared to asymptomatic volunteers (29). So far and to our best knowledge, the diagnostic performance of conventional T2* mapping and UTE-T2* mapping in the assessment of PCL integrity has not been studied.

Thus, our objective was to fill this knowledge gap by aligning both mapping techniques with advanced image post-processing and a model of standardized and graded arthroscopic PCL injury. Our hypotheses were that (I) the condition of the PCL, i.e., intact, partially injured, and completely injured, is reflected by T2* relaxation times

and (II) UTE-T2* mapping is superior to conventional T2* mapping in the assessment of the PCL. We present the following article in accordance with the MDAR checklist (available at <https://qims.amegroups.com/article/view/10.21037/qims-22-251/rc>).

Methods

Study design and sample size estimation

This study was carried out as a prospective, comparative *in-situ* imaging study on human cadaveric knee joint specimens and in adherence to local guidelines and regulations. Power analysis was performed to determine specimen numbers. Based on the initial four specimens [power 0.8; probability of type-I-error 0.01; assumed effect size 1.4 (defined as the mean paired difference divided by the expected standard deviation), two-tailed procedure] and dedicated online software (www.statstodo.com), the minimum sample size was determined as 10. The study was conducted in accordance with the Declaration of Helsinki (as revised in 2013). The study was approved by the Institutional Ethics Committee of Heinrich-Heine-University of Düsseldorf (No. 2019-682) and individual written informed consent was obtained from all subjects involved in the study.

Human cadaveric knee joint specimens

Ten macroscopically intact unfixed and unpaired human knee joint specimens (n=10; right: 4; left: 6) were provided by the local Institute of Anatomy I (Heinrich-Heine-University Düsseldorf, Germany). Seven female and three male specimens were included with a mean age at death of 80.3±7.9 years (range, 64–91 years). Before baseline imaging, the specimens were kept refrigerated at 4 °C and allowed to equilibrate at room temperature for 12 h.

Standardized graded PCL injuries

In-between the MRI measurements, LMW (orthopaedic surgeon with 5 years of experience in arthroscopy) performed standard knee arthroscopies and sequential transections of the PCL as published previously (30). During the first arthroscopy session, the anterolateral and the anteromedial portals were used to access the joint. After identification of the PCL, curved-tip arthroscopic punch forceps (Arthrex®, Naples, FL, USA) were used to carefully synovectomize the PCL for extensive visualization. Partial

PCL injuries were created by performing partial-thickness transections of approximately 50% of the PCL's diameter at the distal-most portion of the ligament not covered by the anterior cruciate ligament (at the transition of the proximal to the central portion of the PCL) using arthroscopic straight-tip scissors (Arthrex®). To emulate *in-vivo* PCL injuries, no particular attention was paid to differentiate the two PCL bundles during transection. The functional integrity of the remaining PCL fibres was confirmed by arthroscopic probing. During the second arthroscopy session, the remaining PCL fibres were completely transected at the same site. After each arthroscopy session, the joint was irrigated to remove air and debris and both portals were sutured. *In vivo*, PCL injuries not only involve tearing of the ligament's fibres and/or bundles but also stretching and elongation. While graded arthroscopic ligament transections were standardized, it is important to note that this model bears only limited resemblance with the PCL injury patterns encountered *in vivo*.

MR image acquisition, post-processing, and analysis

MR image acquisition

Each knee joint underwent sequential MRI measurements in the three PCL conditions (I) intact (PCL_{intact}), (II) following partial PCL transection (PCL_{partial}), and (III) following complete PCL transection (PCL_{complete}). MRI was performed using a clinical-standard 3.0 T MRI scanner (MAGNETOM Prisma, Siemens Healthineers, Erlangen, Germany), a 32-channel spine coil (Spine 32 DirectConnect, Siemens Healthineers), and a flexible 18-channel body coil (Body 18 SlideConnect, Siemens Healthineers) under full coverage of the joint. To standardize specimen position, a dedicated device (30) was used which was not compatible with clinical standard knee coils. Moreover, the specimens were imaged at 90° of flexion which brings the PCL to its greatest length and tension (31) and was intended to reduce partial volume effects and the percentage of PCL fibers oriented at the magic angle. For each specimen and condition, the imaging protocol consisting of morphologic and quantitative sequences (Table 1) was completed. More specifically, clinical-standard T2-weighted (T2w) sequences, a three-dimensional (3D) gradient-echo T2* mapping sequence (henceforth referred to as “conventional T2* mapping”), and density-adapted 3D radial UTE-T2* mapping sequence (32) were acquired along the course of the PCL. Baseline images were used to confirm the absence of any morphologic signs suggestive

Table 1 Acquisition parameters of magnetic resonance sequences

Sequence parameters	T2w	T2w	Conventional T2* mapping	UTE-T2* mapping
Sequence type	2D SE	2D SE	3D GRE	3D GRE
Orientation	parasag (*)	paraxial (*)	parasag (*)	parasag (*)
Repetition time (ms)	864	864	41	19
Echo time (ms)	13	13	4.9/9.8/14.8/19.7/24.6/29.5	0.05/4.0/8.0/12.0/16.0
Field of view (mm × mm)	200×200	200×200	160×160	180×180
Acquisition matrix (pixels)	320×320	320×320	160×160	300×300
Scan percentage (%)	100	100	100	100
Flip angle (°)	155	155	25	6
Number of signal averages (n)			1	
Slices (n)	40	40	72	300
Pixel size (mm/pixel)	0.625×0.625	0.625×0.625	1.0×1.0	0.6×0.6
Slice thickness/gap (mm)	3.0/0.3	3.0/0.3	1.0/0	0.6/0
Duration (min:s)	03:47	03:47	09:53	15:50

(*), aligned along the course of the PCL, i.e., parasagittal and paraxial to the knee joint. T2w, T2-weighted; UTE, ultrashort echo-time; SE, spin-echo; GRE, gradient-echo; parasag, parasagittal.

of prior PCL injury, e.g., fibre disruption and thickening, abnormal ligament configuration or altered signal intensity (12,33). Scanning was performed at room temperature. Magnet time per specimen and condition was approximately 30 min resulting in a total magnet time of approximately 1.5 h per specimen.

MR image post-processing

Using the paintbrush and polygon tools of ITK-SNAP software (v3.8.0, Cognitica, Philadelphia, PA, USA) (34), LMW (clinical radiologist, 5 years of experience in musculoskeletal imaging) performed manual segmentations of the PCL for each specimen and condition. The segmentation outlines of the PCL were delineated on each parasagittal T2* and UTE-T2* image [with echo times of 4.9 ms (conventional T2*) and 12.0 ms (UTE-T2*)] that visualized the PCL. The corresponding T2-weighted images were used for cross reference. Care was taken to exclude borderline voxels at the ligament-fluid interface and, thus, to reduce partial volume effects. As a result, per specimen and condition, the PCL was segmented on 10.1 ± 1.8 (conventional T2*) and 18.1 ± 5.6 (UTE-T2*) images. Segmentation outlines were transferred to the corresponding conventional T2* and UTE-T2* maps. To generate the conventional T2* and UTE-T2*

maps, customized mono-exponential fitting routines were implemented in Python (v3.8.4, Python Software Foundation, Wilmington, DE, USA) and non-linear least-square fits were applied voxel-wise to the exponential decay curves. To validate fit quality, coefficient of determination (R^2) statistics adjusted to the degrees of freedom were calculated, and only voxels with R^2 -values ≥ 0.9 [i.e., $97.1\% \pm 3.6\%$ (UTE-T2*); $96.4\% \pm 4.1\%$ (conventional T2*)] were included in the subsequent analysis.

To assess and quantify regional differences within the PCL, the PCL was further divided into three subregions for additional region-of-interest analysis. To this end, the length of the PCL was automatically determined using 3D centerlines, and the PCL was divided into thirds as published before (18,22) (*Figure 1*). For the PCL_{partial} and PCL_{complete} conditions, the transected ligament portions (i.e., the transection sites) were manually excluded from the segmentation outlines (*Figure 1B,1C*). Consequently, boundary voxels at the proximal and distal borders of the transection sites were excluded to reduce possible partial volume effects secondary to fraying of the PCL stumps and intraligamentous fluid accumulation.

MR image analysis

For each specimen, condition, and principal region-of-

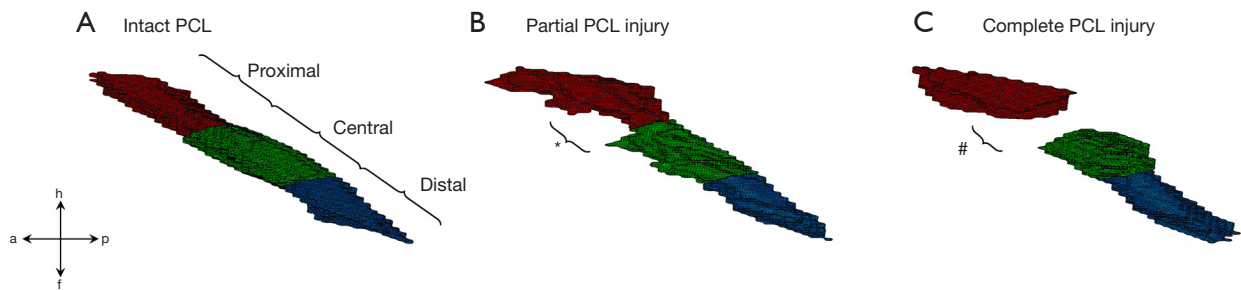


Figure 1 Exemplary 3D visualizations of the PCL and its subregions as a function of PCL condition. Displayed are the intact PCL (A) and the PCL after partial (B) and complete transection (C). Manually segmented outlines of the PCL were automatically divided into thirds, i.e., proximal (red), central (green), and distal (blue). In B, (*) indicates the site of partial transection and the excluded ligament portions, while in C, (#) indicates the completely transected ligament portions. PCL, posterior cruciate ligament; a, anterior; f, feet; h, head; p, posterior.

interest (i.e., the entire ligament and its proximal, central, and distal subregions), T2* relaxation times were determined in a voxel-wise manner. Additionally, texture features were assessed by grey-level co-occurrence matrices (35) to quantify contrast (i.e., homogeneity), orderliness (i.e., energy), and statistical variance of the entire PCL (36,37). Homogeneity indicates similarities between neighbouring pixels and PCL areas with mostly similar (UTE-)T2* values are characterized by high homogeneity values. Energy indicates orderliness and PCL areas with high energy values display similar (UTE-)T2* values and small (UTE-)T2* value differences in neighbouring pixels. Variance measures local variation around the mean and, thus, high variance values indicate high heterogeneity and large differences in (UTE-)T2* values. These features were determined based on routines implemented in MATLAB (R2018b, Natick, MA, USA), four orientations (i.e., 0°, 45°, 90°, and 135°), and an offset of a single voxel (35) for both mapping techniques.

Statistical analysis

Statistical analysis was performed by LMW using GraphPad Prism software (v9.0, San Diego, CA, USA). Voxel numbers were assessed as a function of PCL condition using repeated measures one-way analysis of variance. For conventional and UTE-T2* relaxation times as well as the underlying texture features, normality was assessed using the Shapiro-Wilk test. Normality could not be established and, thus, non-parametric statistical tests were used. Consequently, Friedman's test was used followed by Dunn's multiple comparison test for pairwise *post-hoc* comparisons. To reduce the number of statistically significant, yet clinically irrelevant findings, the level of significance was set to

$P \leq 0.01$. Multiplicity-adjusted p-values are reported to account for the multiple comparisons involved. Data are presented as mean \pm standard deviation.

Results

In the intact condition, fiber discontinuity, abnormal ligament diameter (i.e., thinning or thickening) or signs of ligament degeneration and attrition such as mucoid degeneration or sclerosis were absent in all specimens.

Voxel numbers of entire PCL were characterized by slight, yet significant decreases as a function of PCL injury (conventional T2*: 1,490 \pm 338 voxels (PCL_{intact}); 1,586 \pm 318 voxels (PCL_{partial}); 1,182 \pm 164 voxels (PCL_{complete}); $P=0.002$; UTE-T2*: 7,348 \pm 1,563 voxels (PCL_{intact}); 6,467 \pm 1,426 voxels (PCL_{partial}); 5,579 \pm 797 voxels (PCL_{complete}); $P=0.003$).

In the conventional T2* and UTE-T2* maps, variable and pronounced changes were observed for the entire PCL. In the UTE-T2* maps, relatively low T2* relaxation times were present along the entire length of the PCL when intact (Figure 2A1). With partial PCL injury, the T2* relaxation times were increased in the proximal and central ligament portions (Figure 2A2), while with complete PCL injury, the ligament defect and dehiscence were easily discernible and T2* relaxation time increases were more pronounced and widespread (Figure 2A3). In the conventional T2* maps, the intact PCL displayed homogeneously low T2* relaxation times (Figure 2B1), while the transection sites were characterized by slight increases in T2* relaxation times (Figure 2B2, Figure 2B3): Otherwise, T2* relaxation times remained largely constant despite the increasing extent of the PCL injury. The corresponding UTE-T2* and conventional T2* maps (aligned along the center of

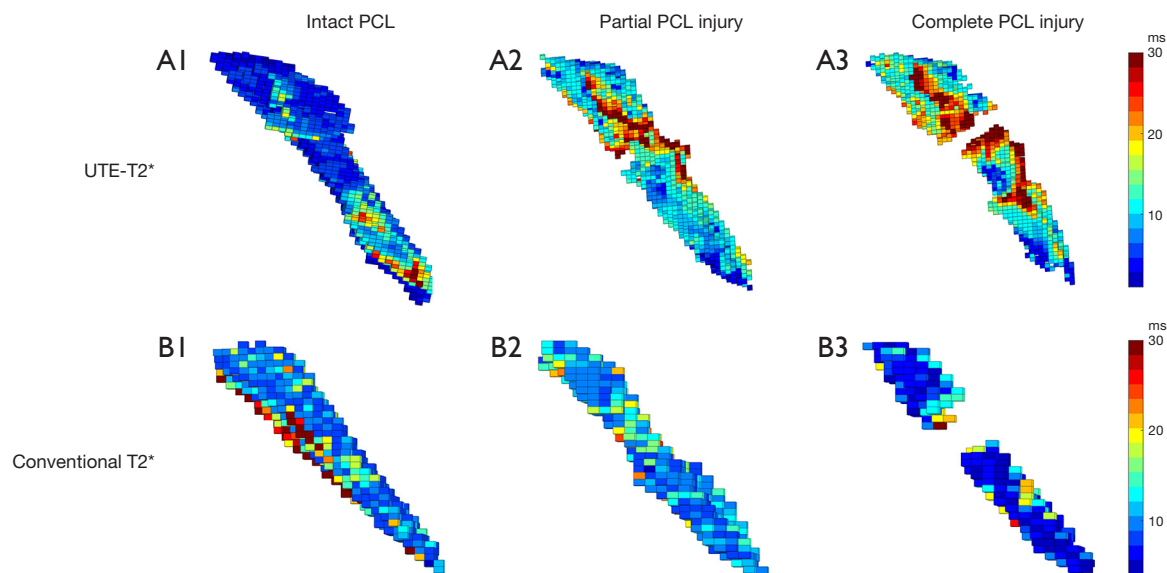


Figure 2 3D volumes of UTE-T2* and conventional T2* maps of the PCL as a function of increasing PCL injury. In this representative knee joint, 3D volumes of spatially resolved quantitative UTE-T2* (A) and conventional T2* (B) maps are displayed in the intact (A1, B1), partially PCL-injured (A2, B2), and completely PCL-injured (A3, B3) conditions. Voxel-wise, T2* relaxation times are color-coded as indicated on the scales on the right that range from 0 to 30 ms. PCL, posterior cruciate ligament; UTE, ultrashort echo-time.

the PCL and overlaid onto the respective 2D morphologic images) are indicated in [Figure S1](#).

These observations were reflected by quantitative changes of the summary statistics and texture features for both UTE-T2* ([Table 2](#)) and conventional T2* ([Table 3](#)).

For UTE-T2*, mean relaxation times of the entire PCL increased significantly with increasing PCL injury, i.e., from 11.1 ± 3.1 ms (PCL_{intact}) to 10.9 ± 4.6 ms (PCL_{partial}) and 14.3 ± 4.9 ms (PCL_{complete}) ($P < 0.001$). *Post-hoc* analyses revealed significant differences between the PCL_{complete} and the PCL_{intact} conditions and subregional analyses indicated significant differences for the proximal and distal subregions. While we observed significant increases for the proximal subregion, from 9.7 ± 4.3 ms (PCL_{intact}) to 12.9 ± 8.1 ms (PCL_{partial}) and 21.3 ± 8.9 ms (PCL_{complete}) ($P \leq 0.001$), we found significant decreases at the distal subregion, from 12.1 ± 3.1 ms (PCL_{intact}) to 8.7 ± 3.2 ms (PCL_{partial}) and 9.8 ± 3.0 ms (PCL_{complete}) ($P < 0.001$). Comparative *post-hoc* analyses indicated significant differences between the PCL_{complete} and the PCL_{intact} conditions (proximal) and the PCL_{partial} and the PCL_{intact} conditions (distal).

For conventional T2*, no significant changes were found for the entire PCL ($P = 0.046$), or the proximal ($P = 0.316$)

and central subregions ($P = 0.222$). For the distal subregion, however, conventional T2* values decreased significantly from 9.6 ± 3.2 ms (PCL_{intact}) to 6.8 ± 2.3 ms (PCL_{partial}) and 7.9 ± 2.7 ms (PCL_{complete}) ($P < 0.001$) and *post-hoc* testing revealed significant differences between the PCL_{partial} and the PCL_{intact} conditions.

For both parameters, texture features over the entire PCL were variable ([Tables 2, 3](#)). Energy values of the UTE-T2* maps decreased significantly with increasing extent of the PCL injury ($P < 0.001$), while energy levels of the conventional T2* maps increased, yet not significantly ($P = 0.710$). Homogeneity remained largely constant and injury-associated changes were not significant, while variance was increased in the UTE-T2* and conventional T2* maps, yet not significantly.

On the voxel level, T2* relaxation times underwent substantially larger changes when assessed using the UTE-T2* versus the conventional T2* mapping sequence ([Figure S2](#)).

Discussion

The most important findings of this study are that (I) UTE-T2* mapping is more responsive to structural damage

Table 2 Quantitative and texture features of UTE-T2* maps of the PCL as a function of PCL condition

UTE-T2* feature	PCL subregion	PCL condition			P value	Post-hoc details		
		Intact PCL	Partial PCL injury	Complete PCL injury		Intact vs. partial	Intact vs. complete	Partial vs. complete
Mean (ms)	Entire	11.1±3.1 (10.6)	10.9±4.6 (8.9)	14.3 ±4.9 (13.0)	<0.001	ns	*	ns
	Subregion							
	Proximal	9.7±4.3 (8.2)	12.9±8.1 (9.2)	21.3±8.9 (20.1)	<0.001	ns	*	ns
	Central	11.4±3.0 (10.6)	10.8±4.1 (9.3)	14.3±4.9 (13.0)	0.012	ns	ns	ns
	Distal	12.1±3.1 (10.9)	8.7±3.2 (7.9)	9.8±3.0 (8.5)	<0.001	**	ns	ns
Energy	Entire	0.09±0.02 (0.09)	0.09±0.02 (0.09)	0.07±0.01 (0.06)	<0.001	ns	*	ns
Homogeneity	Entire	0.13±0.01 (0.13)	0.12±0.01 (0.12)	0.12±0.01 (0.12)	0.064	ns	ns	ns
Variance (ms ²)	Entire	46.7±19.5 (42.0)	53.2±46.0 (34.4)	81.2±53.1 (75.2)	0.187	ns	ns	ns

Mean UTE-T2* relaxation times were determined for the entire PCL and its subregions, while texture variables, i.e., energy, homogeneity, and variance, were quantified for the entire PCL only. Data are mean ± standard deviation. Median values are indicated in parentheses. The UTE-T2* features of the variable PCL conditions (i.e., intact vs. partial vs. complete PCL injury) were compared using Friedman's test followed by Dunn's multiple comparison test. The level of significance of $P \leq 0.01$ (*) was further stratified as $P \leq 0.001$ (**). Significant findings are indicated in *italic*. UTE, ultrashort echo-time; PCL, posterior cruciate ligament; ns, non-significant.

Table 3 Quantitative and texture features of conventional T2* maps of the PCL as a function of PCL condition (please see *Table 2* for details on table organisation and display)

Conventional T2* feature	PCL subregion	PCL condition			P value	Post-hoc details		
		Intact PCL	Partial PCL injury	Complete PCL injury		Intact vs. partial	Intact vs. complete	Partial vs. complete
Mean (ms)	Entire	10.0±3.2 (9.7)	11.4±6.2 (9.5)	15.5±7.8 (14.0)	0.046	ns	ns	ns
	Subregion							
	Proximal	19.1±6.3 (17.7)	17.9±10.0 (14.2)	21.2±15.1 (13.7)	0.316	ns	ns	ns
	Central	11.3±4.0 (10.5)	8.0±2.6 (7.5)	9.1±2.0 (8.6)	0.222	ns	ns	ns
	Distal	9.6±3.2 (8.5)	6.8±2.3 (6.2)	7.9±2.7 (6.9)	<0.001	**	ns	ns
Energy	Entire	0.34±0.08 (0.31)	0.38±0.10 (0.38)	0.37±0.12 (0.34)	0.710	ns	ns	ns
Homogeneity	Entire	0.81±0.03 (0.81)	0.82±0.04 (0.82)	0.81±0.05 (0.80)	0.830	ns	ns	ns
Variance (ms ²)	Entire	57.9±34.4 (58.4)	89.7±74.2 (64.1)	109.1±67.7 (109.0)	0.046	ns	ns	ns

Data are mean ± standard deviation. Median values are indicated in parentheses. The level of significance of $P \leq 0.01$ was further stratified as $P \leq 0.001$ (**). PCL, posterior cruciate ligament; ns, non-significant.

of the PCL (as induced using standardized and graded injuries) than conventional T2* mapping and (II) UTE-T2* mapping may thus assist in differentiating partial PCL injury from complete PCL injury as well as the intact PCL. In addition, this study provides normative values of T2* relaxation times and their underlying texture features for each PCL condition.

For the intact PCL, we determined mean T2* relaxation times of around 11±3 ms (UTE-T2*) and 10±3 ms (conventional T2*). UTE-T2* relaxation times tended to increase from proximal to distal, which confirms earlier findings. Quantifying the UTE-T2* relaxation times of the PCL in asymptomatic volunteers, Okuda *et al.* reported significantly higher mean UTE-T2* relaxation times

in the central and distal subregions of the PCL (38). In contrast, we observed that conventional T2* relaxation times tended to decrease from proximal to distal and that highest T2* relaxation times of 19.1 ± 6.3 ms were present in the proximal subregion. These findings differ from earlier findings by Wilson *et al.* who reported substantially lower T2* relaxation times (of 6–9 ms) in asymptomatic volunteers and did not find any relevant differences between the distinct subregions (22). Potential reasons for these discrepancies involve differences in study design (i.e., *in vivo* vs. *in situ*), joint position (i.e., supine extended vs. lateral flexed), image resolution and sequence parameters as well as scanner and coil specifications. Therefore, inter-study comparisons are challenging, especially in terms of absolute T2* relaxation times. Taken together, these findings confirm the distinctly different profiles of UTE-T2* and conventional T2* mapping sequences. On a physical basis, UTE-T2* sequences capture short T2* signals more efficiently than non-UTE T2* sequences. Consequently, the sensitivity of UTE-T2* mapping towards (ultra-) structural and compositional properties of the collagen network seem higher, simply because both long and short T2* components are detected more efficiently (39). Previous studies of patellar and Achilles tendinopathy demonstrated that T2* mapping sequences were unable to differentiate between intact and injured tendons (25,40,41) and our study confirms these results in the context of the PCL.

For partial PCL injury, slight increases in UTE-T2* relaxation times in the proximal subregion were contrasted by slight-to-pronounced decreases in UTE-T2* relaxation times in the central and distal subregions. In contrast, conventional T2* relaxation times decreased throughout the entire PCL. These changes are most likely reflective of changes in ligament ultrastructure secondary to partial arthroscopic transection and removal of tensioning forces. Once the PCL's fibers are partially disrupted, associated changes such as recoiling, loosening, and reduced macro- and micro-strains likely determine its T2* characteristics. It is important to note that we imaged the knee joint specimens at 90° of flexion, where the PCL is more straightened and pre-strained as compared to full extension or slight knee flexion (42,43) so that -hypothetically- partial PCL injuries may produce more pronounced (ultra-) structural changes. Overall, the significant and concordant decreases in T2* relaxation times at the distal subregion seem to indicate changes of the PCL along its entire length, even though the site of injury was distant and the extent of

injury partial.

For complete PCL injury, we found significant increases in the proximal and non-significant increases in the central subregions for UTE-T2*, while the injury-associated differences were less clear for conventional T2*. Following its complete transection, the stumps of the PCL are damaged, frayed, and disorganized, which is associated with disintegration of the collagen fibrils, loosening of the extracellular matrix, alterations in fiber orientation, and increased influx of water into the tissue, i.e., tissue edema. These concurrent compositional and (ultra-)structural processes are commonly associated with increasing T2* relaxation times (39,44-46). Additionally, complete ligament transections irreversibly alter tissue behavior and structure and bring about crimping, unraveling, and recoiling of the fibrils and fascicles (47). In turn, these changes increase the percentage of fibers oriented at the magic angle of 55° relative to the orientation of the main magnetic field and prolong T2* relaxation times (48,49). Nonetheless, the molecular, compositional, and structural effects of reduced or entirely lost pre-strain and tensile forces across the various scales, i.e., from the level of the collagen microfibril to the fascicle and the entire ligament, and the associated imaging correlates are still poorly understood for the PCL (47), which warrants further research.

By evaluating the spatial distribution of voxel intensities, texture features were analysed to study the underlying ligament structure beyond mere summary statistics (35). Energy provides a measure of textural disorganization. For UTE-T2*, we found significant decreases in energy with increasing PCL injury, which indicates largely different UTE-T2* relaxation times of neighbouring voxels after complete PCL injury (50) and fits in well with the changes outlined above. Corresponding changes were observed for homogeneity and variance that were decreased and increased, respectively. These changes were not statistically significant, most likely due to the substantial standard deviations and limited sample numbers. Consequently, texture features need to be studied more extensively and *in vivo* to determine their potential diagnostic value and clinical contexts for application such as injury, ageing, healing, inflammation, or degeneration.

Even though the experimental PCL injuries were well standardized in the graded injury model, a few limitations must be acknowledged. First, PCL injuries were induced by ligament transection. Because of the surgical approach from anterior, exact standardization of partial transection proved impossible given the limited visualization of the

PCL. Second, PCL injuries as they occur *in vivo* include concurrent processes such as elongation, (over-)stretching, and tearing of the anterolateral and the posteromedial bundles of the PCL (12,22). In our approach, transection of anterior portions of the PCL primarily involved the anterolateral bundle and this injury bears only limited *in-vivo* resemblance. Third, hydrostatic pressure in the knee joint was increased as a result of joint irrigation during arthroscopy and may have artificially increased T2* relaxation times, too (46). Even though the immediate transection sites were manually excluded from the segmentation outlines to counter these effects, this model's clinical transferability is further reduced. Fourth, inflammatory and degenerative processes after ligament rupture, i.e., fibroblast proliferation, angiogenesis, and changes in collagen fiber morphology as signs of incipient healing (51), were not assessed. Consequently, the complex injury patterns of the PCL and the entire joint secondary to clinical PCL injuries cannot be fully emulated *ex vivo*. Nonetheless, such models provide further guidance for subsequent efforts to further refine imaging of partial and complete PCL injuries in patients. Fifth, the PCL status was not referenced histologically or biomechanically. Histologic evaluation of the PCL could help further define the imaging correlates of UTE-T2* and conventional T2*, yet is not the focus of this study. Sixth, the human cadaveric specimens were of advanced age, while the clinical population is younger. To our knowledge, it is not clear how ageing may affect, if at all, the imaging characteristics of the PCL. Seventh, MRI scanning was performed with the joint in 90° of flexion which is unlike the clinical scanning position of 20–30° of flexion and required the use of a flexible multi-channel body coil instead of a dedicated clinical knee coil. While this configuration improved standardization and reduced susceptibility to the magic angle and the partial volume effects (31), clinical transferability of the results may be limited. Eighth, blinding of the reader who performed the segmentation of the PCL was not possible as it was readily discernible on the MR images.

For clinical application, future *in-vivo* studies need to be implemented to corroborate our results by including patients with different PCL pathologies such as partial and complete tears as well as healed, intact, aged, degenerated, and inflammatory ligaments. Our study's clinical setup in terms of a clinical 3T scanner, clinical coils, and clinical sequence parameters allow for immediate translation once regulatory approval is obtained.

Conclusions

This study provides normative values of T2* relaxation times and their underlying texture features based on UTE-T2* and conventional T2* mapping sequences for the PCL and its distinct subregions as a function of ligament condition. In contrast to conventional T2* mapping, UTE-T2* mapping captures short T2* signals and allows quantitative assessment of ligament (ultra-) structure and integrity that may help to improve diagnostic differentiation. Once further substantiated beyond the *in-situ* setting, UTE-T2* mapping may refine non-invasive evaluation of PCL injuries and enhance clinical decision-making as well as monitoring of treatment outcome. Other potential applications include monitoring of ligament healing and functional assessment of the PCL in clinical questions related to ageing, degeneration and/or inflammation.

Acknowledgments

We would like to express our gratitude to Sabine Wittschonke and Marco Warten (Institute for Anatomy I, Heinrich-Heine-University Düsseldorf, Germany) for anatomical preparation of the human knee joint specimens. *Funding:* This work was supported by the local Research Committee of the Medical Faculty of Heinrich-Heine-University Düsseldorf, Germany and the Deutsche Forschungsgemeinschaft (DFG) (No. NE 2136/3-1).

Footnote

Reporting Checklist: The authors have completed the MDAR checklist. Available at <https://qims.amegroups.com/article/view/10.21037/qims-22-251/rc>

Conflicts of Interest: All authors have completed the ICMJE uniform disclosure form (available at <https://qims.amegroups.com/article/view/10.21037/qims-22-251/coif>). The authors have no conflicts of interest to declare.

Ethical Statement: The authors are accountable for all aspects of the work in ensuring that questions related to the accuracy or integrity of any part of the work are appropriately investigated and resolved. The study was conducted in accordance with the Declaration of Helsinki (as revised in 2013). The study was approved by

the Institutional Ethics Committee of Heinrich-Heine-University of Düsseldorf (No. 2019-682) and individual written informed consent was obtained from all subjects involved in the study.

Open Access Statement: This is an Open Access article distributed in accordance with the Creative Commons Attribution-NonCommercial-NoDerivs 4.0 International License (CC BY-NC-ND 4.0), which permits the non-commercial replication and distribution of the article with the strict proviso that no changes or edits are made and the original work is properly cited (including links to both the formal publication through the relevant DOI and the license). See: <https://creativecommons.org/licenses/by-nc-nd/4.0/>.

References

- Logan M, Williams A, Lavelle J, Gedroyc W, Freeman M. The effect of posterior cruciate ligament deficiency on knee kinematics. *Am J Sports Med* 2004;32:1915-22.
- Strobel MJ, Weiler A, Schulz MS, Russe K, Eichhorn HJ. Arthroscopic evaluation of articular cartilage lesions in posterior-cruciate-ligament-deficient knees. *Arthroscopy* 2003;19:262-8.
- Gao SG, Jiang W, Lei GH, Xu M, Yu F, Li KH. Effect of posterior cruciate ligament rupture on biomechanical features of the medial femoral condyle. *Orthop Surg* 2011;3:205-10.
- Arøen A, Sivertsen EA, Owesen C, Engebretsen L, Granan LP. An isolated rupture of the posterior cruciate ligament results in reduced preoperative knee function in comparison with an anterior cruciate ligament injury. *Knee Surg Sports Traumatol Arthrosc* 2013;21:1017-22.
- Parkar AP. Imaging the Anterior and Posterior Cruciate Ligaments. *J Belg Soc Radiol* 2016;100:98.
- Naraghi A, White LM. MR imaging of cruciate ligaments. *Magn Reson Imaging Clin N Am* 2014;22:557-80.
- Bedi A, Musahl V, Cowan JB. Management of Posterior Cruciate Ligament Injuries: An Evidence-Based Review. *J Am Acad Orthop Surg* 2016;24:277-89.
- Laoruengthana A, Jarusriwana A. Sensitivity and specificity of magnetic resonance imaging for knee injury and clinical application for the Naresuan University Hospital. *J Med Assoc Thai* 2012;95 Suppl 10:S151-7.
- DePhillipo NN, Cinque ME, Godin JA, Moatshe G, Chahla J, LaPrade RF. Posterior Tibial Translation Measurements on Magnetic Resonance Imaging Improve Diagnostic Sensitivity for Chronic Posterior Cruciate Ligament Injuries and Graft Tears. *Am J Sports Med* 2018;46:341-7.
- Patten RM, Richardson ML, Zink-Brody G, Rolfe BA. Complete vs partial-thickness tears of the posterior cruciate ligament: MR findings. *J Comput Assist Tomogr* 1994;18:793-9.
- Tewes DP, Fritts HM, Fields RD, Quick DC, Buss DD. Chronically injured posterior cruciate ligament: magnetic resonance imaging. *Clin Orthop Relat Res* 1997;(335):224-32.
- Rodriguez W Jr, Vinson EN, Helms CA, Toth AP. MRI appearance of posterior cruciate ligament tears. *AJR Am J Roentgenol* 2008;191:1031.
- Servant CT, Ramos JP, Thomas NP. The accuracy of magnetic resonance imaging in diagnosing chronic posterior cruciate ligament injury. *Knee* 2004;11:265-70.
- Kam CK, Chee DW, Peh WC. Magnetic resonance imaging of cruciate ligament injuries of the knee. *Can Assoc Radiol J* 2010;61:80-9.
- Jung YB, Jung HJ, Yang JJ, Yang DL, Lee YS, Song IS, Lee HJ. Characterization of spontaneous healing of chronic posterior cruciate ligament injury: Analysis of instability and magnetic resonance imaging. *J Magn Reson Imaging* 2008;27:1336-40.
- Wilson KJ, Frupp J, Lockard CA, Shin RC, Engstrom C, Ho CP, LaPrade RF. Quantitative mapping of acute and chronic PCL pathology with 3 T MRI: a prospectively enrolled patient cohort. *J Exp Orthop* 2019;6:22.
- Ranmuthu CDS, MacKay JW, Crowe VA, Kaggie JD, Kessler DA, McDonnell SM. Quantitative analysis of the ACL and PCL using T1rho and T2 relaxation time mapping: an exploratory, cross-sectional comparison between OA and healthy control knees. *BMC Musculoskelet Disord* 2021;22:916.
- Wilms LM, Radke KL, Abrar DB, Latz D, Schock J, Frenken M, Windolf J, Antoch G, Filler TJ, Nebelung S. Micro- and Macroscale Assessment of Posterior Cruciate Ligament Functionality Based on Advanced MRI Techniques. *Diagnostics (Basel)* 2021;11:1790.
- Beveridge JE, Machan JT, Walsh EG, Kiapour AM, Karamchedu NP, Chin KE, Proffen BL, Sieker JT, Murray MM, Fleming BC. Magnetic resonance measurements of tissue quantity and quality using T2* relaxometry predict temporal changes in the biomechanical properties of the healing ACL. *J Orthop Res* 2018;36:1701-9.
- Williams AA, Titchenal MR, Andriacchi TP, Chu CR. MRI UTE-T2* profile characteristics correlate to walking mechanics and patient reported outcomes 2

- years after ACL reconstruction. *Osteoarthritis Cartilage* 2018;26:569-79.
21. Crețu A, Mattea C, Stapf S. Low-field and variable-field NMR relaxation studies of H₂O and D₂O molecular dynamics in articular cartilage. *PLoS One* 2021;16:e0256177.
 22. Wilson KJ, Surowiec RK, Ho CP, Devitt BM, Fripp J, Smith WS, Spiegl UJ, Dornan GJ, LaPrade RF. Quantifiable Imaging Biomarkers for Evaluation of the Posterior Cruciate Ligament Using 3-T Magnetic Resonance Imaging: A Feasibility Study. *Orthop J Sports Med* 2016;4:2325967116639044.
 23. Biercevicz AM, Miranda DL, Machan JT, Murray MM, Fleming BC. In Situ, noninvasive, T2*-weighted MRI-derived parameters predict ex vivo structural properties of an anterior cruciate ligament reconstruction or bioenhanced primary repair in a porcine model. *Am J Sports Med* 2013;41:560-6.
 24. Biercevicz AM, Murray MM, Walsh EG, Miranda DL, Machan JT, Fleming BC. T2 * MR relaxometry and ligament volume are associated with the structural properties of the healing ACL. *J Orthop Res* 2014;32:492-9.
 25. Kijowski R, Wilson JJ, Liu F. Bicomponent ultrashort echo time T2* analysis for assessment of patients with patellar tendinopathy. *J Magn Reson Imaging* 2017;46:1441-7.
 26. Warth RJ, Zandiyeh P, Rao M, Gabr RE, Tashman S, Kumaravel M, Narayana PA, Lowe WR, Harner CD. Quantitative Assessment of In Vivo Human Anterior Cruciate Ligament Autograft Remodeling: A 3-Dimensional UTE-T2* Imaging Study. *Am J Sports Med* 2020;48:2939-47.
 27. Breda SJ, de Vos RJ, Poot DHJ, Krestin GP, Hernandez-Tamames JA, Oei EHG. Association Between T2 * Relaxation Times Derived From Ultrashort Echo Time MRI and Symptoms During Exercise Therapy for Patellar Tendinopathy: A Large Prospective Study. *J Magn Reson Imaging* 2021;54:1596-605.
 28. Robson MD, Gatehouse PD, So PW, Bell JD, Bydder GM. Contrast enhancement of short T2 tissues using ultrashort TE (UTE) pulse sequences. *Clin Radiol* 2004;59:720-6.
 29. Hayashi S, Nakasa T, Matsuoka Y, Akiyama Y, Ishikawa M, Nakamae A, Awai K, Adachi N. Evaluation of the degenerative pattern of PCL in osteoarthritis patients using UTE-T2 mapping. *Asia Pac J Sports Med Arthrosc Rehabil Technol* 2021;24:35-40.
 30. Wollschläger LM, Radke KL, Schock J, Kotowski N, Latz D, Kanschik D, Filler TJ, Caspers S, Antoch G, Windolf J, Abrar DB, Nebelung S. The MRI posterior drawer test to assess posterior cruciate ligament functionality and knee joint laxity. *Sci Rep* 2021;11:19687.
 31. Craddock W, Smithers T, Harris C, du Moulin W, Molnar R. Magnetic resonance imaging of the posterior cruciate ligament in flexion. *Knee* 2018;25:507-12.
 32. Nagel AM, Laun FB, Weber MA, Matthies C, Semmler W, Schad LR. Sodium MRI using a density-adapted 3D radial acquisition technique. *Magn Reson Med* 2009;62:1565-73.
 33. LaPrade CM, Civitarese DM, Rasmussen MT, LaPrade RF. Emerging Updates on the Posterior Cruciate Ligament: A Review of the Current Literature. *Am J Sports Med* 2015;43:3077-92.
 34. Yushkevich PA, Piven J, Hazlett HC, Smith RG, Ho S, Gee JC, Gerig G. User-guided 3D active contour segmentation of anatomical structures: significantly improved efficiency and reliability. *Neuroimage* 2006;31:1116-28.
 35. Haralick RM, Shanmugam K, Dinstein I. Textural Features for Image Classification. *IEEE Trans Syst Man Cybern* 1973;SMC-3:610-21.
 36. Lambin P, Rios-Velazquez E, Leijenaar R, Carvalho S, van Stiphout RG, Granton P, Zegers CM, Gillies R, Boellard R, Dekker A, Aerts HJ. Radiomics: extracting more information from medical images using advanced feature analysis. *Eur J Cancer* 2012;48:441-6.
 37. Joseph GB, Baum T, Carballido-Gamio J, Nardo L, Virayavanich W, Alizai H, Lynch JA, McCulloch CE, Majumdar S, Link TM. Texture analysis of cartilage T2 maps: individuals with risk factors for OA have higher and more heterogeneous knee cartilage MR T2 compared to normal controls--data from the osteoarthritis initiative. *Arthritis Res Ther* 2011;13:R153.
 38. Okuda M, Kobayashi S, Toyooka K, Yoshimizu R, Nakase J, Hayashi H, Ueda Y, Gabata T. Quantitative differentiation of tendon and ligament using magnetic resonance imaging ultrashort echo time T2* mapping of normal knee joint. *Acta Radiol* 2021. [Epub ahead of print].
 39. Williams A, Qian Y, Bear D, Chu CR. Assessing degeneration of human articular cartilage with ultra-short echo time (UTE) T2* mapping. *Osteoarthritis Cartilage* 2010;18:539-46.
 40. Juras V, Apprich S, Szomolanyi P, Bieri O, Deligianni X, Trattig S. Bi-exponential T2 analysis of healthy and diseased Achilles tendons: an in vivo preliminary magnetic resonance study and correlation with clinical score. *Eur Radiol* 2013;23:2814-22.
 41. Grosse U, Syha R, Hein T, Gatidis S, Grözinger G, Schabel C, Martirosian P, Schick F, Springer F. Diagnostic

- value of T1 and T2* relaxation times and off-resonance saturation effects in the evaluation of Achilles tendinopathy by MRI at 3T. *J Magn Reson Imaging* 2015;41:964-73.
42. Li G, DeFrate LE, Sun H, Gill TJ. In vivo elongation of the anterior cruciate ligament and posterior cruciate ligament during knee flexion. *Am J Sports Med* 2004;32:1415-20.
 43. Rao Z, Zhou C, Kernkamp WA, Foster TE, Bedair HS, Li G. In vivo kinematics and ligamentous function of the knee during weight-bearing flexion: an investigation on mid-range flexion of the knee. *Knee Surg Sports Traumatol Arthrosc* 2020;28:797-805.
 44. Gatehouse PD, Bydder GM. Magnetic resonance imaging of short T2 components in tissue. *Clin Radiol* 2003;58:1-19.
 45. Williams A, Qian Y, Golla S, Chu CR. UTE-T2* mapping detects sub-clinical meniscus injury after anterior cruciate ligament tear. *Osteoarthritis Cartilage* 2012;20:486-94.
 46. Gold GE, Han E, Stainsby J, Wright G, Brittain J, Beaulieu C. Musculoskeletal MRI at 3.0 T: relaxation times and image contrast. *AJR Am J Roentgenol* 2004;183:343-51.
 47. Zitnay JL, Weiss JA. Load transfer, damage, and failure in ligaments and tendons. *J Orthop Res* 2018;36:3093-104.
 48. Bydder M, Rahal A, Fullerton GD, Bydder GM. The magic angle effect: a source of artifact, determinant of image contrast, and technique for imaging. *J Magn Reson Imaging* 2007;25:290-300.
 49. Shao H, Pauli C, Li S, Ma Y, Tadros AS, Kavanaugh A, Chang EY, Tang G, Du J. Magic angle effect plays a major role in both T1rho and T2 relaxation in articular cartilage. *Osteoarthritis Cartilage* 2017;25:2022-30.
 50. Truhn D, Zwingenberger KT, Schock J, Abrar DB, Radke KL, Post M, Linka K, Knobe M, Kuhl C, Nebelung S. No pressure, no diamonds? - Static vs. dynamic compressive in-situ loading to evaluate human articular cartilage functionality by functional MRI. *J Mech Behav Biomed Mater* 2021;120:104558.
 51. Nayak M, Nag HL, Nag TC, Digge V, Yadav R. Ultrastructural and histological changes in tibial remnant of ruptured anterior cruciate ligament stumps: a transmission electron microscopy and immunochemistry-based observational study. *Musculoskelet Surg* 2020;104:67-74.

Cite this article as: Wilms LM, Radke KL, Latz D, Thiel TA, Frenken M, Kamp B, Filler TJ, Nagel AM, Müller-Lutz A, Abrar DB, Nebelung S. UTE-T2* versus conventional T2* mapping to assess posterior cruciate ligament ultrastructure and integrity—an *in-situ* study. *Quant Imaging Med Surg* 2022;12(8):4190-4201. doi: 10.21037/qims-22-251

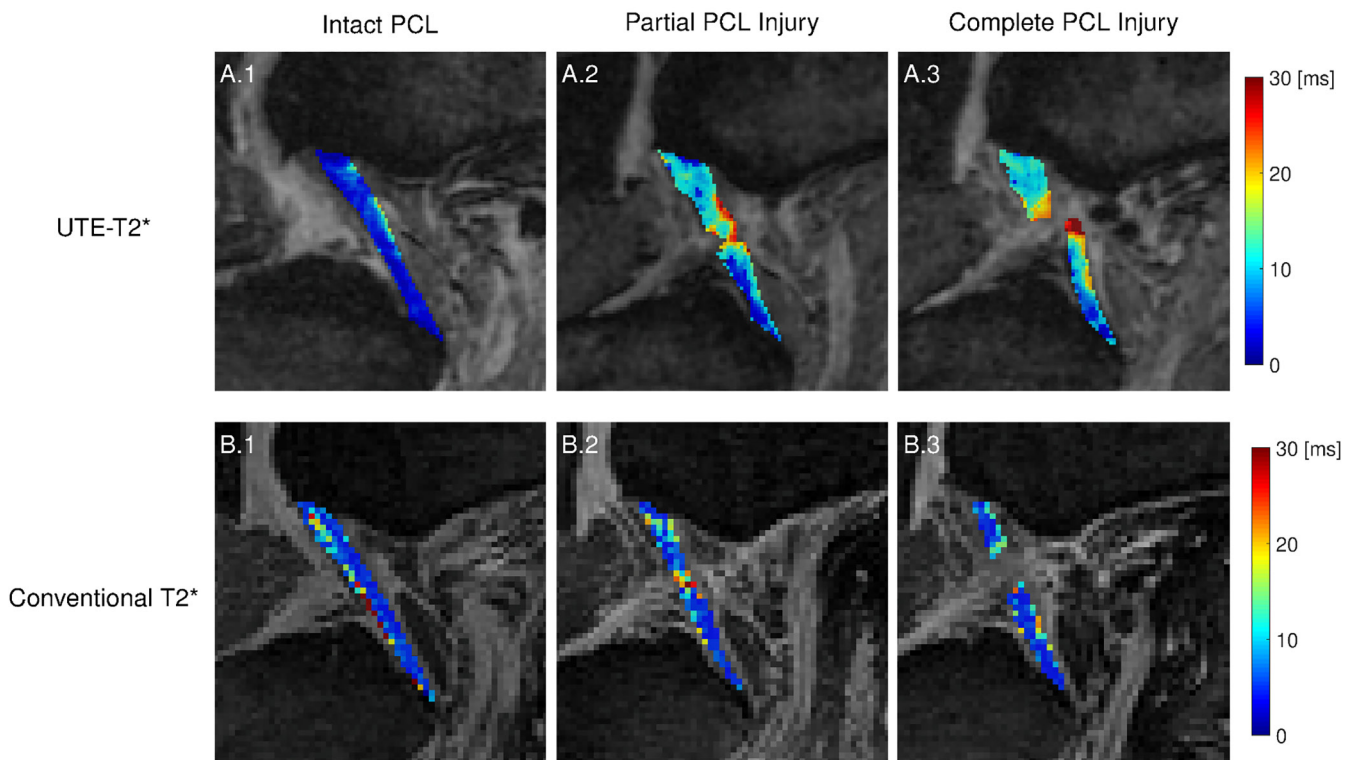


Figure S1 2D UTE-T2* and conventional T2* maps of the PCL as a function of its condition. In this representative knee joint, spatially resolved quantitative UTE-T2* maps (A) and conventional T2* maps (B) of the central PCL are displayed in the intact (A1, B1), partially PCL-injured (A2, B2), and completely PCL-injured (A3, B3) conditions. UTE-T2* maps and conventional T2* maps were overlaid onto the corresponding morphologic images with echo times of 12.0 ms [UTE-T2*] and 4.9 ms [conventional T2*]. Pixel-wise, T2* relaxation times are color-coded and range from 0 to 30 ms. Same knee joint as in *Figure 2*. PCL, posterior cruciate ligament.

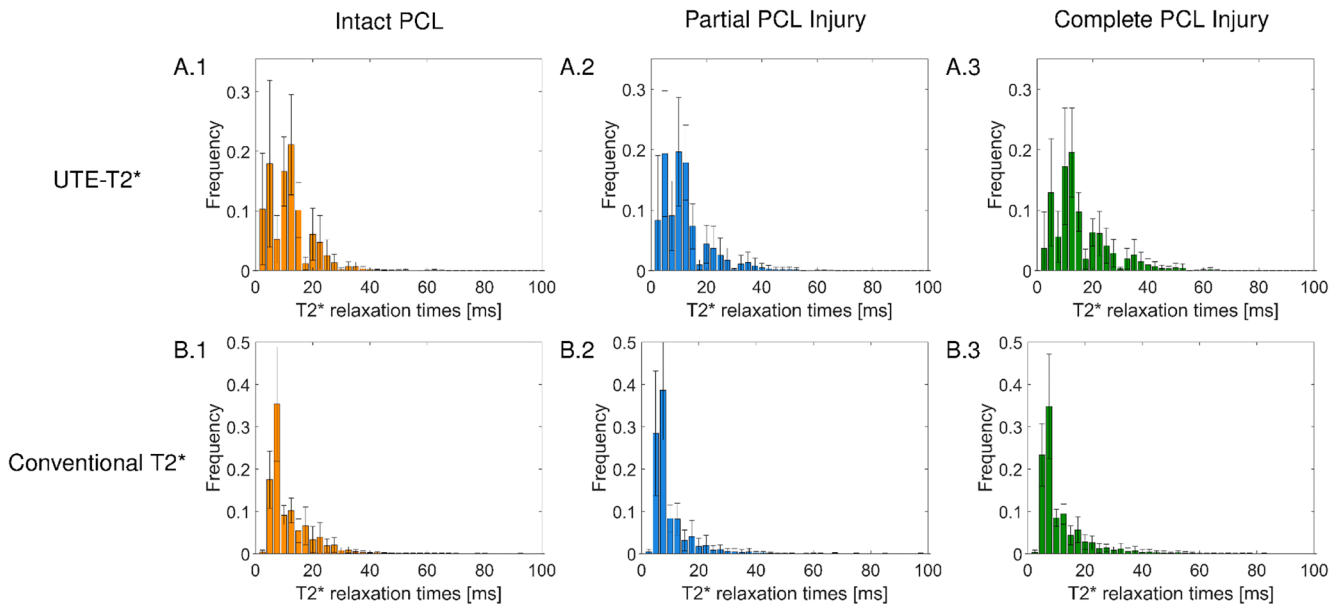


Figure S2 Histograms of individual voxels' T2* relaxation times as acquired using the UTE-T2* and conventional T2* sequences as a function of PCL condition. Displayed are the frequencies of individual voxels' T2* relaxation times in all specimens. T2* relaxation times are scaled at intervals of 2.5 ms. Bars indicate means, while whiskers indicate standard deviations. Intact (A1, B1), partially PCL-injured (A2, B2), and completely PCL-injured (A3, B3) conditions. PCL, posterior cruciate ligament.